Preprints.org

Article

Not peer-reviewed version

Anti-Diabetic Potential of the American Mistletoe *Phoradendron brachystachyum*: In Vitro and In Silico Approach

Luis Aurelio Montoya-Inzunza , Lennin Isaac Garrido-Palazuelos , José Roberto Aguirre-Sánchez , Erika Ortega-Hernández , J. Basilio Heredia , Jose Reyes Gonzalez-Galaviz , Pedro de Jesús Bastidas-Bastidas , José Andrés Medrano-Félix , Luis Angel Cabanillas-Bojórquez , Marilena Antunes-Ricardo * , Erick Paul Gutiérrez-Grijalva *

Posted Date: 27 March 2026

doi: 10.20944/preprints202603.2241.v1

Keywords: phytochemicals; oxidative stress; flavonoids; diabetes; insulin resistance

Preprints.org is a free multidisciplinary platform providing preprint service that is dedicated to making early versions of research outputs permanently available and citable. Preprints posted at Preprints.org appear in Web of Science, Crossref, Google Scholar, Scilit, Europe PMC.

Copyright: This open access article is published under a Creative Commons CC BY 4.0 license, which permit the free download, distribution, and reuse, provided that the author and preprint are cited in any reuse.

Preprints.org (www.preprints.org) | NOT PEER-REVIEWED | Posted: 27 March 2026 doi:10.20944/preprints202603.2241.v1

Disclaimer/Publisher's Note: The statements, opinions, and data contained in all publications are solely those of the individual author(s) and contributor(s) and not of MDPI and/or the editor(s). MDPI and/or the editor(s) disclaim responsibility for any injury to people or property resulting from any ideas, methods, instructions, or products referred to in the content.

Article

Anti-Diabetic Potential of the American Mistletoe *Phoradendron brachystachyum*: In Vitro and In Silico Approach

Luis Aurelio Montoya-Inzunza [1,2], Lennin Isaac Garrido-Palazuelos [3], José Roberto Aguirre-Sánchez [4], Erika Ortega-Hernández [5], J. Basilio Heredia [2], Jose Reyes Gonzalez-Galavis [6], Pedro de Jesús Bastidas-Bastidas [2], José Andrés Medrano Félix [7], Luis Angel Cabanillas-Bojórquez [8], Marilena Antunes-Ricardo [5,9,*] and Erick Paul Gutiérrez-Grijalva [7,10,*]

[1] Unidad de Investigaciones en Biotecnología Biomédica. Universidad Autónoma de Occidente, UR Culiacán. Blvd. Lola Beltrán y Blvd. Rolando Arjona, 4 de marzo, 80020, Culiacán, Sinaloa, México

[2] Centro de Investigación en Alimentación y Desarrollo, A.C., Carretera a Eldorado Km. 5.5, Col. Campo El Diez, CP. 80110, Culiacán, Sinaloa, México

[3] Departamento Académico de Ciencias de la Salud, Universidad Autónoma de Occidente, Unidad Regional Los Mochis. Blvd. Macario Gaxiola y Carretera Internacional, México 15, C.P. 81223, Los Mochis, Sinaloa, México

[4] Laboratorio Nacional para la Investigación en Inocuidad Alimentaria (LANIIA). Centro de Investigación en Alimentación y Desarrollo A.C. (CIAD) Unidad Culiacán, Sinaloa, México

[5] Centro de Biotecnología FEMSA, Escuela de Ingeniería y Ciencias, Tecnológico de Monterrey, Av. Eugenio Garza Sada 2501 Sur, Monterrey, NL, 64849, México

[6] Programa de Investigadoras e Investigadores por México SECIHTI-Instituto Tecnológico de Sonora, Ciudad Obregón 85000, Sonora, México

[7] Programa de Investigadoras e Investigadores por México SECIHTI-Centro de Investigación en Alimentación y Desarrollo, A.C., Carretera a Eldorado Km. 5.5, Col. Campo El Diez, CP.80110, Culiacán, México

[8] Posdoc SECIHTI - Centro de Investigación en Alimentación y Desarrollo, A.C., Carretera a Eldorado Km. 5.5, Col. Campo El Diez, CP. 80110, Culiacán, México

[9] Institute for Obesity Research Monterrey, Tecnológico de Monterrey, Av. Eugenio Garza Sada 2501 Sur, C.P. 64849 Monterrey, NL, México

[10] Centro de Investigación y Docencia en Ciencias de la Salud, Universidad Autónoma de Sinaloa, Culiacán, CP 80030, Sinaloa, México

* Correspondence: marilena.antunes@tec.mx (M.A.R.); erick.gutierrez@ciad.mx (E.P.G.G.)

Abstract

The anti-diabetic potential of *Phoradendron brachystachyum* was evaluated through the assessment of the cellular antioxidant, anti-inflammatory, and glucose uptake-modulating activities of its non-digested (ND) and digested (D) extracts from leaves (L), stems (S), and whole aerial parts (WAP). The WAP non-digested extract exhibited the highest cellular antioxidant activity, with a 99% inhibition of reactive oxygen species in Caco-2 cells, and a significant reduction in nitric oxide production in RAW 264.7 cells. Crucially, in an insulin-resistant HepG2 cell model, the WAP extract significantly increased glucose consumption to 82.67%, retaining high bioactivity (66.55%) even after the digestion process. UPLC-MS analysis identified quercetin-3-O-rhamnoside as the most abundant in all extracts. Complementary the in silico molecular docking and 100 ns molecular dynamics simulations identified spiraeoside and quercetin-3-O-alpha-L-rhamnopyranoside as potent α-glucosidase inhibitors (-9.9kcal mol^{-1}), while sakuranetin and spiraeoside showed higher affinity for α-amylase (-9.0 kcal mol^{-1}). These in vitro and in silico findings provide a scientific basis for the ethnopharmacological use *P. brachystachyum*, showing its potential to modulate glucose metabolism.

© 2026 by the author(s). Distributed under a Creative Commons CC BY license.

Preprints.org (www.preprints.org) | NOT PEER-REVIEWED | Posted: 27 March 2026 doi:10.20944/preprints202603.2241.v1

Keywords: phytochemicals; oxidative stress; flavonoids; diabetes; insulin resistance

1. Introduction

Diabetes mellitus is a non-communicable disease (NCD) characterized by elevated blood glucose levels; when untreated, it can cause permanent damage to liver cells involved in glucose regulation, and to the cells of the pancreas that produce insulin [1]. In 2024, the International Diabetes Federation estimated that there were 13.6 million Mexicans with type 2 diabetes (over 20 years old) [2]. Some of the most common causes for the development of this pathology are associated with obesity/overweight, poor diet, genetic factors, and a sedentary lifestyle. Furthermore, other factors related to the onset of diabetes and its complications are linked to oxidative stress. Oxidative stress is generated by an imbalance in the levels of antioxidant compounds and reactive oxygen species (ROS); the increase in these oxidizing compounds, particularly the superoxide radical, causes damage to different macromolecules such as lipids, proteins, and DNA, affecting the integrity and functions of the cell. Additionally, increased ROS levels are associated with a stronger inflammatory response, leading to the overproduction of nitric oxide, which favors the development of atherosclerosis and, in turn, causes multiple complications, such as insulin resistance [3–5]. There are several drugs and treatments for diabetes; however, their adverse effects, such as hypoglycemia, weight gain, and abdominal pain, among others, represent an important issue in public health [6,7]. In this regard, several studies have focused on the empirical use of plants by the population for the treatment of diabetes and related conditions, such as hyperlipidemia and elevated serum glucose levels [8]. Mexico has a diverse range of medicinal plants used ethnobotanically in traditional medicine to treat various diseases. However, it is necessary to conduct studies to provide scientific evidence about the presence of bioactive compounds, their properties, and mechanisms of action, which explain how they exert their specific function [9]. Plant-derived phytochemicals, including glycosides, alkaloids, phenolic compounds, terpenes, flavonoids, and carotenoids, have been studied and shown to have anti-diabetic potential due to their antioxidant and anti-inflammatory activities in cell lines and animals. Additionally, their effects on lowering insulin resistance have been observed in cell lines and animals [10]. A multi-target strategy is often desired for diabetes management, not only to control postprandial hyperglycemia but also to mitigate systemic insulin resistance by enhancing insulin sensitization in peripheral tissues, such as the liver, to stimulate glucose uptake from the blood. , but also modulating the oxidative stress and the systemic and sustained inflammation that give rise to these clinical manifestations and persist, creating a vicious cycle, as well as modifying carbohydrate metabolism to reduce its impact on the glycemic index by inhibiting digestive enzymes, such as α-glucosidase and α-amylase, which delay carbohydrate hydrolysis and glucose absorption. Thus, research is needed to identify natural compounds that can modulate these pathways, offering alternatives to synthetic drugs. Mistletoes are aerial hemiparasitic plants that grow in different species of gymnosperms and angiosperms; they are considered pests since they feed on their host, thus affecting their development [11]. Toji (*Phoradendron brachystachyum*) is a species of mistletoe belonging to the family Santalaceae, distributed from the southern United States to northern Mexico, and has been traditionally used for the treatment of hyperlipidemia and diabetes [12]. Traditionally, different species of mistletoe have been used to treat cancer, hyperlipidemia, and diabetes. There is a growing interest in the study of these mistletoes and their beneficial properties for health, within which antioxidant, analgesic, hypoglycemic, and lipid-lowering properties have been reported; this is due to compounds content in them naturally, such as phenolic compounds like epicatechin, epicatechin gallate, naringenin, catechin, procyanidin B1, quercetin and luteolin [13–15]. It is important to mention that this polyphenolic compounds has a low bioaccessibility due to the digestion processes in the gastrointestinal tract, causing alterations in their structure or degrading, so evaluating the bioaccessibility of the compounds present in Toji extracts after subjecting them to oral, gastric and intestinal conditions will give us valuable information about which and where the compounds that manage to resist the digestive process exert their bioactivity [16,17]. In a recent study

© 2026 by the author(s). Distributed under a Creative Commons CC BY license.

Preprints.org (www.preprints.org) | NOT PEER-REVIEWED | Posted: 27 March 2026 doi:10.20944/preprints202603.2241.v1

by Gutiérrez-Grijalva, et al. [18], they evaluated the bioaccessibility of Toji compounds obtained via in vitro digestion, with values ranging from 7.78% to 22.60% for ferulic acid, quinic acid, gallic acid, coumaric acid, and caffeic acid. However, cell permeability in the intestinal monolayer has not been evaluated, nor has the inhibition of nitric oxide production, cellular antioxidant activity, and cellular insulin utilization been examined to observe the decrease in insulin resistance.

This work aimed to provide scientific evidence about the anti-diabetic potential of leaf (L), stem (S), and whole aerial parts (WAP) extracts from *Phoradendron brachystachyum* using an in vitro and in silico approach to evaluate their impact on oxidative stress, inflammation, insulin-resistance, and carbohydrate metabolism, physiological processes frequently altered in individuals with type 2 diabetes.

2. Materials and Methods

2.1. Plant Material

The mistletoe (*P. brachystachyum*) was collected in July 2021 in Guamúchil, Sinaloa (25°44′42″N, 108°05′38″W), which was parasitizing mesquite trees (*Prosopis juliflora*). The plants were identified in the herbarium Jesús González Ortega of the Faculty of Agronomy of the UAS (FA-UAS-022352 and 013284). The plant parts were classified into leaves, stems, and aerial parts (leaf and stem combined). They were then washed with chlorinated water at 50 ppm and allowed to dry at 40°C for 48 hours in a forced-air convection drying oven. The dried samples were recovered, and leaf, stem, and aerial parts were ground separately in a Turf brand coffee mill until a fine powder was obtained. The dust was sieved at 600 µm, collected in plastic airtight bags, and sealed in cellophane bags to prevent moisture from entering the sample.

2.2. Extraction of Phytochemicals

A methanol extraction was carried out according to Gutiérrez-Grijalva, et al. [19] with some modifications. Briefly, 0.5 g of the mistletoe powder sample was mixed with 10 mL of methanol: water (8:2 v/v) solution and stirred for 2 h at 100 rpm. Subsequently, the samples were centrifuged (HERMLE Labortechnik GmbH type Z 36 HK and 221.22 rotor) at 10,000 rpm at 4 °C for 15 min, and the methanol part was evaporated. The water supernatant from the extract was recovered, and the solvent was freeze-dried; the weight of the dry extract was determined. The dry extract (0.02 g) was resuspended in 2 mL of 80% methanol to obtain a known concentration. The extracts were prepared in triplicate (n = 3).

2.3. Static Simulated Digestion Assay

The digestion assay was performed based on Brodkorb, et al. [17], as shown in **Table S2**. In 50 mL tubes, 0.02 g of lyophilized plant sample was added. *Oral phase*: 1.6 mL of salivary phase, calcium chloride (10 µL), α-amylase (0.2 mL), and distilled water (0.19 mL) were mixed and incubated for 2 min at 37 ° C in a stirrer. *Gastric phase*: In the same test tube, 3.2 mL of gastric phase was added, and the pH was regulated to 3 using sodium hydroxide or 1M hydrochloric acid, calcium chloride (2 µL) pepsin (0.2 mL), lipase (0.2 mL, recheck pH to 3), distilled water (398 µL) and incubate for 2 h at 37 ° C in stirring. *Intestinal phase*: 4.4 mL of intestinal phase was added in the same test tube, pH was measured and regulated to 7, calcium chloride (16 µL), pancreatin (2 mL, recheck the pH to 7), and distilled water (1,584 mL) were added, and incubated for 2 hours at 37 ° C under stirring. Finally, the test tubes were recovered, immersed in boiling water for 45 sec to inactivate the enzyme, centrifuged at 10 rpm, 4 ° C for 15 min to recover the digest supernatant, and filtered through 0.45 µM Acrodiscs. The filtrate was dried in a Vacuum evaporator (EZ-2.3, Genevac Ltd., Ipswich, EN, USA) for 2 h to remove the small methanol fraction, leaving only the water fraction; after this, the water fraction was frozen at -80 °C for 2 h. Once frozen, the water fractions were freeze-dried and weighed to obtain the dry weight of the digested extract.

© 2026 by the author(s). Distributed under a Creative Commons CC BY license.

Preprints.org (www.preprints.org) | NOT PEER-REVIEWED | Posted: 27 March 2026 doi:10.20944/preprints202603.2241.v1

2.4. Biological Evaluation of P. brachystachyum Methanolic Extracts

2.4.1. Cell Viability in RAW 264.7, Caco-2, and HepG2 Cells

Human colorectal adenocarcinoma Caco-2 cells (ATCC® HTB-37™, Manassas, VA, USA), human hepatocellular carcinoma (HepG2) cells (ATCC® HB-8065™), and mouse macrophages RAW 264.7 cells (ATCC® TIB-71™) were obtained from the American Type Culture Collection (ATCC®, Manassas, VA, USA). Human cells (Caco-2 and HepG2) were cultured in Dulbecco's Modified Eagle Medium (DMEM) supplemented with 5% fetal bovine serum (FBS) and 1% Pen-Strep (GIBCO, Carlsbad, CA, USA) antibiotic in 5% in a humidified atmosphere containing 5% CO_2 at 37 °C, whereas mouse macrophages (RAW 264.7) cells were cultured in DMEM supplemented with 10% FBS and 1% Pen-Strep antibiotic at same conditions.

2.4.2. Cellular Antioxidant Activity (CAA)

Cellular antioxidant activity of non-digested and digested extracts of *P. brachystachyum* was evaluated in Caco-2 cells as a human colon model according to the method described by Meléndez-Martínez, et al. [20] Cell viability of Caco-2 cells treated with different concentrations (25-100 µg/mL) of samples was assessed using CellTiter 96® Aqueous One Solution Cell Proliferation Assay (Promega, Madison, WI, USA). After that, cells were seeded in a 96-well plate (5×10^4 cells/well) and incubated for 24 hours. After, cells were treated with 100 µL of samples (25µg/mL) containing 60 µM 2′,7′-dichlorodihydrofluorescein diacetate (DCFH-DA). Then, cells were incubated for 60 min at 37 °C. After incubation, treatments were removed and the cells were washed twice with phosphate-buffered saline (PBS). Finally, 100 µL of a 500 µM solution of 2,2′-azobis-2-methylpropanimidamide dihydrochloride (AAPH) was added to each well, except for the blank and negative control wells. Fluorescence at 538 nm, excited at 485 nm, was measured every 2 minutes for 90 minutes at 37 °C using a microplate reader. CAA values were calculated using the following equation 1:

$$\text{CAA Unit} = 1 - (\int SA / \int CA) \quad (1)$$

where $\int SA$ is the integrated area under the sample fluorescence versus time curve, and $\int CA$ is the integrated area from the control curve.

2.4.3. Glucose Uptake in an Insulin-Resistant (IR) Cell Model of HepG2 Cells

The effect of non-digested and digested extracts of *P. brachystachyum* on glucose uptake using an insulin-resistant model was performed following that reported by Meléndez-Martínez, et al. [20]. Human hepatic (HepG2) cells were grown in DMEM medium supplemented with 5% FBS and 1% Pen-Strep (GIBCO, Carlsbad, CA, USA) and maintained at 37 °C in a humidified atmosphere of 5% CO_2. After seeding 5 x 10^4 cells/well in a 96-well plate and incubating for 24 h, the medium was changed to high-glucose (25 mM D-glucose) DMEM. After that, half of the wells were treated with 50 µL of human insulin (Sigma-Aldrich, St. Louis, MO, USA) to achieve a final concentration of 5 × 10−7 mol/L and induce insulin resistance, while the other half served as a control. After 24 hours, the medium was replaced with fresh media containing 25 µg/mL of non-digested and digested samples, and the samples were incubated for 5 hours. Glucose content in the media was measured using the Glucose (GO) assay kit (Sigma-Aldrich, MO, USA) according to the manufacturer's instructions. Absorbance was measured at 540 nm in a microplate reader (Synergy HT, Bio-Tek, Winooski, VT, USA). Cells not treated with insulin or any treatment were considered the non-insulin-resistant or normal control (CTRL Normal), and cells treated with insulin but without treatment were considered the insulin-resistance control (CTRL IR). Commercial glibenclamide (200 µM) was used as a reference drug. Glucose consumption was expressed as a percentage of glucose uptake (%).

© 2026 by the author(s). Distributed under a Creative Commons CC BY license.

Preprints.org (www.preprints.org) | NOT PEER-REVIEWED | Posted: 27 March 2026 doi:10.20944/preprints202603.2241.v1

2.4.4. Nitric Oxide Inhibition Assay

The anti-inflammatory potential of *P. brachystachyum* digested and non-digested extracts was evaluated through the determination of nitric oxide production following the method described by Meléndez-Martínez, et al. [20]. Cells were seeded at 5 ×10^4 cells/well in a 96-well plate and incubated for 24 h. After that, different concentrations (25-100 µg/mL) of undigested and digested extracts of *P. brachystachyum* were added and incubated for four hours. Then, half of the wells were activated with lipopolysaccharide (LPS, 1µg/mL) (*Escherichia coli* O127B8 , Sigma-Aldrich, MA, USA), whereas the other half was used as a control for each sample. The production of nitric oxide (NO) was determined in the culture supernatants by measuring nitrite concentration using the Griess reagent system (Promega, Madison, WI, USA) according to the manufacturer's instructions. After incubation, the absorbance values were read at 550 nm on a Synergy HT plate reader (Bio-Tek Instruments, Inc., VT, USA). The NO concentration was calculated by comparison with a sodium nitrite standard (0.39–50 µM) curve and considering the cell viability of the original plate measured as described in *section 2.4.2.* Results were expressed as the percentage of inhibition of nitric oxide production.

2.4.6. Determination of Phenolic Compounds Content by UPLC-MS

The flavonoid content in the *P. brachystachyum* extracts was evaluated based on the methodology described by Picos-Salas, et al. [21] using a UPLC class H (Waters Corporation, USA) coupled to a G2-XS QT mass-mass spectrometer analyzer (Quadrupole and Time of Flight). Flavonoids were separated using a UPLC BEH C18 column (1.7 µm × 2.1 mm × 100 mm) at 40 °C. Gradient elution was conducted with water-formic acid 0.1% (A) and acetonitrile (B) at a flow rate of 0.3 mL/min. The following gradient was used: 0 min, 95% (A); 5 min, 70% (A); 9 min, 30% (A); 14 min, 0% (A); 14.5 min, 0% (A); 15 min, 95% (A); and 16 min, 95% (A). Electrospray (ESI) was used for compound ionization, and the mass analysis condition was: capillary voltage of 1.5 kV, sampling cone of 30 V, desolvation gas of 800 L/h, and a temperature of 500 °C. A 0–30 V collision ramp was used. The flavonoids were identified and quantified by comparing them with a calibration curve using the corresponding standards of quercetin, apigenin-8-O-glucoside, apigenin, quercetin-3-O-rhamnoside, luteolin, luteolin-7-glucoside, naringenin, naringin, formononetin, genistein, mangiferin, rutin, hesperidin, kaempferol, phloretin, phloridzin, and circimaritin.

2.5. In Silico Evaluations

2.5.1. Selection of the Target Receptors and 3D Structure Retrieval

The digestive enzymes α-amylase and α-glucosidase were selected as molecular targets for the in silico analyses due to their central role in carbohydrate metabolism, postprandial glucose regulation, and the development of insulin resistance, as well as their relevance to the bioaccessibility and biological activity of dietary polyphenols. The crystallographic structure of α-amylase (1B2Y) and α-glucosidase was retrieved from the Protein Data Bank (https://www.rcsb.org/). In contrast, since no experimentally resolved structure of α-glucosidase was available in public structural databases, it three-dimensional structure was generated by homology using the SWISS-Model web server (https://swissmodel.expasy.org/) [22,23] The amino acid sequence of α-glucosidase from *Saccharomyces cerevisiae* (UniProt ID: P53341) was obtained from the UniProt database (https://www.uniprot.org/) as described by Khan, et al. [24] and Taha, et al. [25]. The 3D structures of the receptors were visualized using Discovery Studio v2021 (**Figure S1**).

2.5.2. In Silico Selection and Retrieval of P. brachystachyum Compounds

A total of 14 phytochemical compounds previously identified in *P. brachystachyum*, were selected as ligands for the in silico interaction analyses with the target enzymes. These compounds were chosen based on prior phytochemical and metabolomic reports describing their presence in the species and their potential biological relevance. The chemical structures of all selected compounds

© 2026 by the author(s). Distributed under a Creative Commons CC BY license.

Preprints.org (www.preprints.org) | NOT PEER-REVIEWED | Posted: 27 March 2026 doi:10.20944/preprints202603.2241.v1

were retrieved from the PubChem database (https://pubchem.ncbi.nlm.nih.gov/), including their canonical SMILES notation, molecular weight (MW), and molecular formula (**Table S1**). Three-dimensional structures of the ligands were downloaded in SDF format and converted to PDB format using Discovery Studio v2021, for further analysis.

2.5.3. Drug-Likeness, PASS Analysis, ADMET Properties, and Toxicity of the P. brachystachyum Compounds

An in silico pharmacokinetic and safety profile of the selected P. brachystachyum compounds was performed to evaluate their drug-likeness, predicted biological activity, and ADMET properties (absorption, distribution, metabolism, excretion, and toxicity). Drug-likeness and ADMET parameters were predicted using the SwissADME web server (https://swissadme.ch/) (Daina et al., 2017), with particular emphasis on Lipinski's Rule of Five, which considers key molecular descriptors such as molecular weight, lipophilicity, hydrogen bond donors and acceptors, and polar surface area. Prediction of Activity Spectra for Substances (PASS) analysis was conducted using the PASS Online platform available through the Way2Drug server (https://way2drug.com/PassOnline/). This tool predicts the probability of a compound exhibiting specific biological activities based on its chemical structure and known structure–activity relationships, expressed as the probabilities of activity (Pa) and inactivity (Pi). PASS analysis was employed to explore the potential pharmacological profiles of the selected compounds, including enzyme inhibition, receptor modulation, and other bioactivities relevant to metabolic disorders.

Additionally, toxicity risk assessment was carried out using the ProTox-II (Protox 3.0) web server (https://tox.charite.de/protox3/index.php?site=home), which predicts possible adverse effects and assigns toxicity classes based on established quantitative structure–activity relationship (QSAR) models. This integrated in silico evaluation provided an initial assessment of the pharmacological feasibility and safety profile of the investigated compounds prior to molecular docking and dynamic simulation studies.

2.5.4. Molecular Docking of P. brachystachyum and the Receptors α-Glucosidase and α-Amylase

Molecular docking analyses were performed to investigate the binding interactions between selected *P. brachystachyum* compounds and the carbohydrate-hydrolyzing enzymes α-glucosidase and α-amylase. Docking simulations were conducted using AutoDock Tools version 1.5.6. Prior to docking, the receptor structures were prepared by the addition of polar hydrogen atoms, assignment of Gasteiger and Kollman partial charges, and conversion to the PDBQT format. Ligand structures were similarly prepared by charge assignment, addition of polar hydrogens, and conversion to PDBQT format to ensure compatibility with the docking protocol. Grid boxes were defined to encompass the active sites of both enzymes in order to guide ligand sampling within the catalytically relevant regions. A grid box size of 40 × 40 × 40 points along the x, y, and z axes, with a grid spacing of 0.375 Å, was employed to allow comprehensive exploration of the binding pocket. The grid box center coordinates for α-glucosidase were set at x = 0.941, y = 3.360, and z = −0.103, while those for α-amylase were defined at x = 8.428, y = 59.265, and z = 18.831. Binding affinities were estimated based on the calculated binding free energies, expressed in kcal·mol^{-1}, with more negative values indicating stronger predicted ligand–receptor interactions.

2.5.5. Molecular Dynamics Simulation

Molecular dynamics (MD) simulations were performed to evaluate the conformational stability and interaction dynamics of the four selected protein–ligand complexes: α-amylase in complex with sakuranetin and spiraeoside, and α-glucosidase in complex with quercetin 3-O-α-L-rhamnopyranoside and spiraeoside. All simulations were carried out using GROMACS version 2018 with the CHARMM27 force field.[26]. Each protein–ligand complex was placed at the center of a triclinic simulation box and solvated using the TIP3P water model, maintaining a minimum distance

© 2026 by the author(s). Distributed under a Creative Commons CC BY license.

Preprints.org (www.preprints.org) | NOT PEER-REVIEWED | Posted: 27 March 2026 doi:10.20944/preprints202603.2241.v1

of 1.0 nm between the solute and the box boundaries. System electroneutrality was achieved by the addition of appropriate counterions (Na^+ and Cl^-). Energy minimization was conducted using the steepest descent algorithm with a maximum of 50,000 steps to eliminate unfavorable steric contacts. Following minimization, the systems were equilibrated under constant number, volume, and temperature (NVT) conditions and subsequently under constant number, pressure, and temperature (NPT) conditions, each for 100 ps. Production MD simulations were then performed for 100 ns for each complex under periodic boundary conditions. Trajectory analyses were conducted to assess structural stability and flexibility by calculating the root mean square deviation (RMSD), root mean square fluctuation (RMSF), radius of gyration (Rg), and potential energy over the simulation time. All graphical analyses were generated and processed using XMGrace.

3. Results

3.1. Quantification of Polyphenols Present in Non-Digested and Digested Extracts of Phoradendron brachystachyum by UPLC-MS

The chromatographic analysis of the non-digested (ND) and digested (D) extracts of *P. brachystachyum* showed the presence of quercetin-3-O-rhamnoside, rutin, and hesperidin, where quercetin-3-O-rhamnoside was the most abundant in both digested and non-digested extracts (Table 1). The low concentrations of rutin and hesperidin, and the absence of other compounds, may be due to degradation and structural transformations induced by interactions with digestive enzymes and changes in pH [27,28].

Table 1. Quantification of polyphenols present in non-digested (ND) and digested (D) extracts of *P. brachystachyum* by UPLC-MS.

Retention time (min)	m/z [M-H]-	Compound	Leaf (µg/dry weight extract)		Stem (µg/dry weight extract)		Aerial parts (µg/dry weight extract)	
			Non-digested	Digested	Non-digested	Digested	Non-digested	Digested
3.73	449.10056145	Quercetin-3-O-rhamnoside	1355.59 ± 142.88 ^{c}	115.63 ± 12.41 ^{d}	3605.11 ± 436.24 ^{a}	529.28 ± 27.17 ^{d}	2901.26 ± 213.15 ^{b}	198.16 ± 23.98 ^{d}
3.31	611.15338487	Rutin	260.75 ± 26.87 ^{a}	0 ^{c}	50.81 ± 3.10 ^{b}	0^{c}	275.85 ± 19.34 ^{a}	0^{c}
3.31	611.18977037	Hesperidin	243.94 ± 19.34 ^{a}	0 ^{b}	0 ^{b}	0 ^{b}	264.14 ± 25.05 ^{a}	0 ^{b}
Total polyphenol content			1,860.28	115.63	3,655.92	529.28	3,441.25	198.16

Data shown as mean ± standard deviation, three replicates with three repetitions per replication. ^{abc} Different letters indicate significant differences by Tukey's test ($p < 0.05$) per compound.

3.2. Cellular Antioxidant Activity (CAA)

The assay of cellular antioxidant activity was carried out in the Caco2 cell line, evaluating the non-digested and digested extracts of the leaves (L), stems (S), and whole aerial parts (WAP) of *P. brachystachyum*. Cell viability assessment showed that both non-digested and digested samples exhibited viability greater than 80% at 25 µg/mL (**Figure S2**). Non-digested and digested samples did not show significant differences in cell viability for any of the extracts analyzed. Still, a slight increase in cell viability was observed in digested samples. This tendency to greater viability or less cytotoxicity in cellular tissues by digested extracts may be because when undergoing a digestion process, the content of compounds of the extracts undergoes modifications caused by the effect of pH

© 2026 by the author(s). Distributed under a Creative Commons CC BY license.

Preprints.org (www.preprints.org) | NOT PEER-REVIEWED | Posted: 27 March 2026 doi:10.20944/preprints202603.2241.v1

change in each of the digestive phases, the possible interaction with digestive enzymes, thus causing deprotonation, degradation and possible hydrolysis of phenolic compounds, so they become less cytotoxic to cell tissue [16,17,29–33]. The cell viability value was significantly reduced to 75% and 58% when the concentrations were increased to 50 and 100 µg/mL, respectively. Therefore, 25 µg/mL was selected as an appropriate concentration for the subsequent assay.

As shown in **Figure 1**, at the concentration evaluated (25 µg/mL) the non-digested extracts were those that had greater antioxidant activity as exhibit leaf (L), stem (S), and whole aerial parts (WAP) extracts which exhibited an inhibition on the production of intracellular reactive oxygen species (ROS) by 93.30%, 95.99%, and 99.00%, respectively. No significant differences were observed between the antioxidant activity of non-digested and digested leaf (L) or stem (S) extracts. Although no significant differences in cellular antioxidant capacity are observed when using leaves and stems together in the whole aerial parts extract compared to using them independently, a tendency toward increased antioxidant activity is observed. Only digested whole aerial parts (WAP) showed a significant reduction (93.20%) in the cellular antioxidant with respect to non-digested WAP extracts. This can be attributed to the fact that the structures of compounds change as they pass through different pH levels and interact with various enzymes during the oral, gastric, and intestinal phases, which, in most cases, leads to the degradation of the cellular antioxidant activity of phytochemicals [33]. These results can be compared with previous studies by Junaid, et al. [34], which reported cellular antioxidant activity, measured as inhibition of peroxyl radical formation by 76%, attributing this activity to the presence of sakuranetin, one of its major compounds in the methanolic extracts of *Phoradendron robinsonii*. This is important because this compound has already been identified in metabolomic studies of *P. brachystachyum*. The cellular antioxidant activity of different flavonoids has been reported, where flavonoids such as quercetin, galangin, kaempferol, epigallocatechin 3-gallate (EGCG), epicatechin-3-gallate (ECG), luteolin, morin, myricetin, quercetin-3-glucoside, epigallocatechin, catechin, epicatechin, and taxifolin have presented cellular antioxidant activity. The path of flavonoids through the different metabolic phases of digestion until they reach the enterocytes, for further absorption and transport to the different tissues, affects the structure and capacity of the compounds [35]. It is reported that three structural features are essential in these compounds to carry out their antioxidant activity: 1) a B-ring o-dihydroxy group, 2) a 2,3-double bond combined with 3) a 4-oxo group in the C-ring, hydroxyl groups, as well as quercetin glycosylation and structures similar to isoflavones and flavanols [36]. According to the literature, a fundamental characteristic for flavonoids to exert cellular antioxidant activity is the presence of a 3′, 4′-dihydroxy group, especially in flavonoids that do not belong to the subclass of flavonols, as previously reported, the presence of a catechol group in the B ring [37,38].

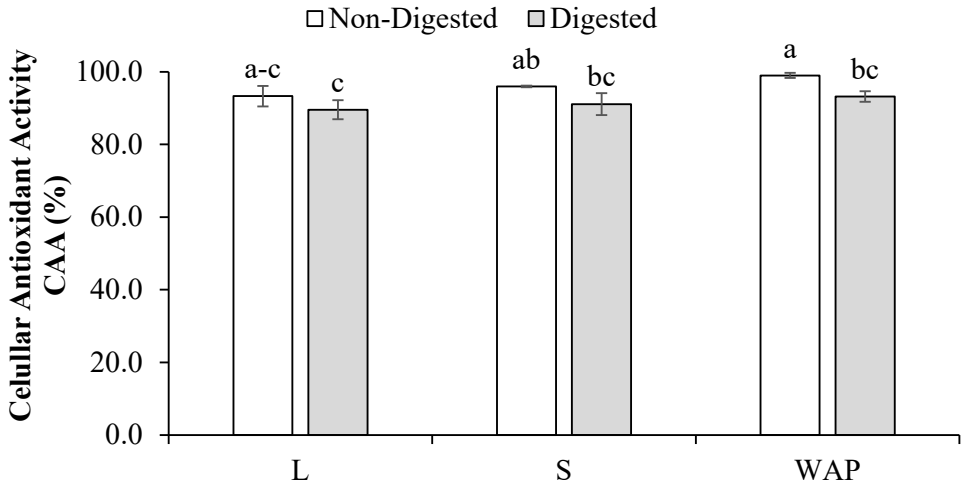

© 2026 by the author(s). Distributed under a Creative Commons CC BY license.

Preprints.org (www.preprints.org) | NOT PEER-REVIEWED | Posted: 27 March 2026 doi:10.20944/preprints202603.2241.v1

Figure 1. Cellular antioxidant activity, CAA (%), in the human colorectal adenocarcinoma (Caco2) cells treated with leaf (L), stem (S), and whole aerial parts (WAP) extracts from *P. brachystachyum,* before (non-digested) and after (digested), submitted to a simulated gastrointestinal digestion. Samples were evaluated at a concentration of 25 μg/mL. Data shown as mean ± standard deviation [abc] Different letters indicate significant differences between samples determined by Tukey's test ($p < 0.05$).

3.3. Glucose Uptake in an Insulin-Resistant (IR) Cell Model of HepG2 Cells

HepG2 cells are a liver cell line widely used to assess cellular glucose utilization in vitro in models of insulin resistance [39]. Insulin resistance in insulin-sensitive organs leads to a state of hyperglycemia, hyperinsulinemia, and hypertriglyceridemia, which are standard features of type 2 diabetes. Insulin resistance in liver cells impairs glycogen synthesis, thereby failing to suppress glucose production, and is the most significant contributor to hyperglycemia [4]. The impact on cell viability of HepG2 cells by leaf (L), stem (S), and whole aerial parts (WAP) of *P. brachystachyum* extracts on the cell viability of HepG2 cells was evaluated (**Figure S3**) Non-digested extracts exhibited cell viabilities ranging between 85%-93% when assessed at 25 μg/mL, where the leaf (L) extracts showed the lower cell viability percentages (85.83%). Digested extracts did not show any negative impact on cell viability at the same concentrations. When the extract concentrations were increased to 50 and 100 μg/mL, a dramatic reduction in cell viability was observed for all three *P. brachystachyum* extracts, reaching values as low as 54.52% of the viability observed with WAP extracts at 100 μg/mL. Likewise, at these doses, a significant reduction in cell viability was observed in cells treated with non-digested extracts compared to those treated with digested extracts. Considering these results, 25 μg/mL was selected as an appropriate concentration for the subsequent assay.

The glucose consumption assay was performed in the HepG2 cell line, evaluating non-digested and digested extracts of leaf (L), stem (S), and whole aerial parts (WAP) of *P. brachystachyum,* comparing them with an insulin-resistant non-treated control, a normal non-treated control, and glibenclamide as a reference drug (**Figure 2**). Although there is no significant statistical difference between the three non-digested extracts and between the three digested extracts, the greatest percentage of glucose consumption occurred in the cells treated with the extract of whole aerial parts (WAP), both in its non-digested extract (82.67%) and digested extract (66.55%) regarding the leaf (L) and stem (S) extracts.

We could hypothesize that the difference in glucose utilization improvement between non-digested and digested extracts may be due to the degradation of compounds responsible for bioactivity during different gastric phases, which could consequently decrease their bioactivity [40]. Although digested extracts show a reduced ability to reverse insulin resistance compared to non-digested extracts, they still exhibit higher glucose utilization than the control in the insulin-resistant model (35.18%), indicating some improvement. The increase in glucose uptake induced by leaf (L), stem (S), and whole aerial parts (WAP) of *P. brachystachyum* extracts in insulin-resistant cells was comparable to that observed in cells treated with glibenclamide (200 μM). It is a commercial drug of reference indicated for individuals with diabetes, which improves glucose transport and increases glucose uptake in these cells.

These results can be compared with those obtained by Roghani and Baluchnejadmojarad [41], where they reported an increase in hepatic glucose consumption by the presence of epicatechin gallate in a mouse model of induced diabetes, as well as in a study by Huang, et al. [4], where the presence of quercetin increased hepatic glucose consumption, reporting that the presence of quercetin in mouse adipocytes blocks insulin-stimulated effects on glucose metabolism, including glucose transport, oxidation and incorporation into lipids, mentioning that an active receptor tyrosine kinase is necessary to mediate these effects [42]. Also, research conducted by Nomura, et al. [43] demonstrated that flavonoids such as luteolin, quercetin, apigenin, and kaempferol inhibited insulin signaling in mouse fat cells by suppressing insulin receptor phosphorylation and subsequent inhibition of Akt activation.

© 2026 by the author(s). Distributed under a Creative Commons CC BY license.

Preprints.org (www.preprints.org) | NOT PEER-REVIEWED | Posted: 27 March 2026 doi:10.20944/preprints202603.2241.v1

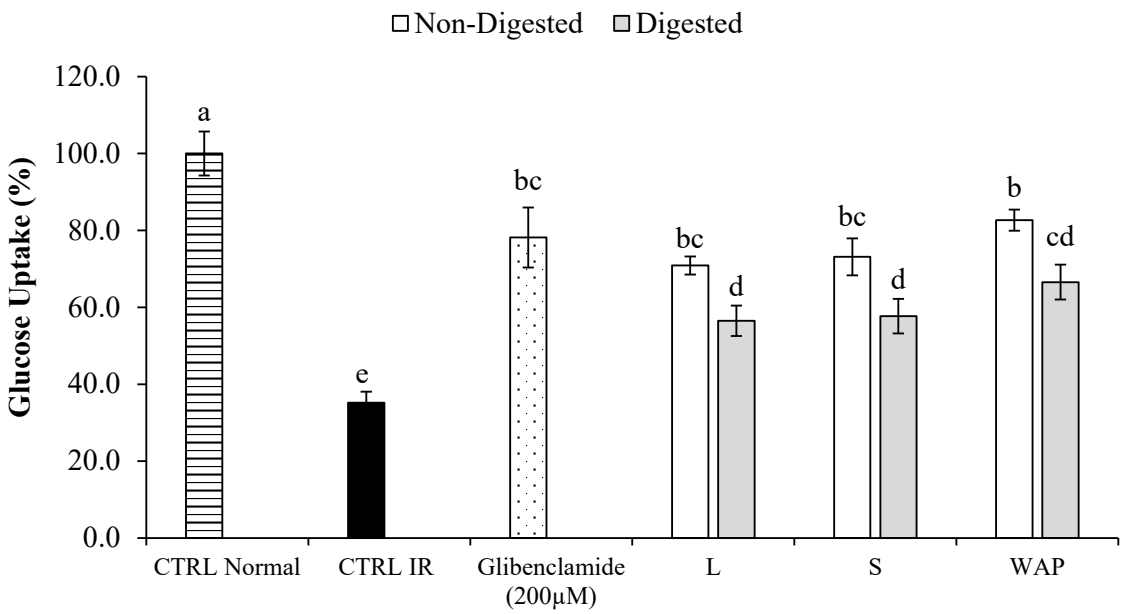

Figure 2. Glucose uptake (%) using an insulin-resistant model induced in human hepatic (HepG2) cells treated with leaf (L), stem (S), and whole aerial parts (WAP) extracts from *P. brachystachyum*, before (non-digested) and after (digested), submitted to a simulated gastrointestinal digestion. Samples were evaluated at a concentration of 25 µg/mL. Data shown as mean ± standard deviation [abc] Different letters indicate significant differences between samples determined by Tukey's test ($p < 0.05$). CTRL Normal: Cells non-insulin-resistant or normal control; CTRL IR: Insulin-resistant cells without treatment. Glibenclamide (200 µM) was used as a reference drug.

3.4. Nitric Oxide Inhibition Assay

The nitric oxide inhibition test was performed in the RAW 264.7 cell line, evaluating the non-digested and digested extracts of the leaf (L), stem (S), and whole aerial parts (WAP) of *P. brachystachyum*. The viability of RAW 264.7 cells treated with 25 µg/mL of *P. brachystachyum* extracts was higher than 88%. All three extracts from non-digested extracts reduced nitric oxide production by up to 13%. Notably, whole aerial parts (WAP) exhibited the most pronounced inhibition (**Figure 3).** No significant differences in the inhibition of nitric oxide production were observed between non-digested and digested samples on any of the three extracts. These results agree with Orhan, et al. [44] who obtained an inhibition of nitric oxide of 37.08% by methanolic extracts of *Viscum album*; it has also been reported that the presence of compounds such as procyanidin B1, which has been reported present in metabolomic analyses of the species *P. brachystachyum* activates anti-inflammatory signals ERK (extracellular signal-regulated kinases), suppressing pro-inflammatory genes and transcription factors such as nuclear factor-kappa B (NF-κB) [45]. Some studies report that epigallocatechin gallate (EGCG) inhibits the activation of pro-inflammatory transcription factors such as Nf-κB induced by lipopolysaccharide (LPS) by inhibiting the degradation of IκB kinase (IKK). Procyanidins-rich extract has also been reported to inhibit p65 translocation to the nucleus, iNOS expression, and nitric oxide production in RAW cells 264.7 [46]. Inhibition of human IKK activity has also been reported as an important target in the anti-inflammatory potential of procyanidins, and their effectiveness is closely related to their structure. LPS induces oxidative stress in cells, leading to increased production of nitric oxide and reactive oxygen species in macrophages [47]. It is well known that ROS are related to intracellular signaling. [48] Procyanidins, as potent antioxidants, can prevent increased production of ROS, which is associated with the activation of the signaling system of the transcription factor Nf-κB [49,50] and the mitogen-activated protein kinase (MAPK) signaling pathway [51]. In the same way, the literature provides evidence of reciprocal communication between the ERK and Nf-κB

© 2026 by the author(s). Distributed under a Creative Commons CC BY license.

Preprints.org (www.preprints.org) | NOT PEER-REVIEWED | Posted: 27 March 2026 doi:10.20944/preprints202603.2241.v1

pathways, hypothesizing that ERK activates Nf-κB, which could explain how procyanidins could inhibit both pathways [52–54]. Also in monocytes, the main source of reactive oxygen species induced by activation of Nf-κB has been the complex nicotinamide adenine dinucleotide phosphate (NADPH) oxidase [55,56]; thus, inhibition of NADPH oxidase by procyanidins could be responsible for this effect [57]. Other possible mechanisms by which these compounds exert this effect include inhibition of the LPS response through neutralization and direct binding to LPS molecules [58,59], some dimeric procyanidins may act by inhibiting Nf-κB by binding to DNA [60].

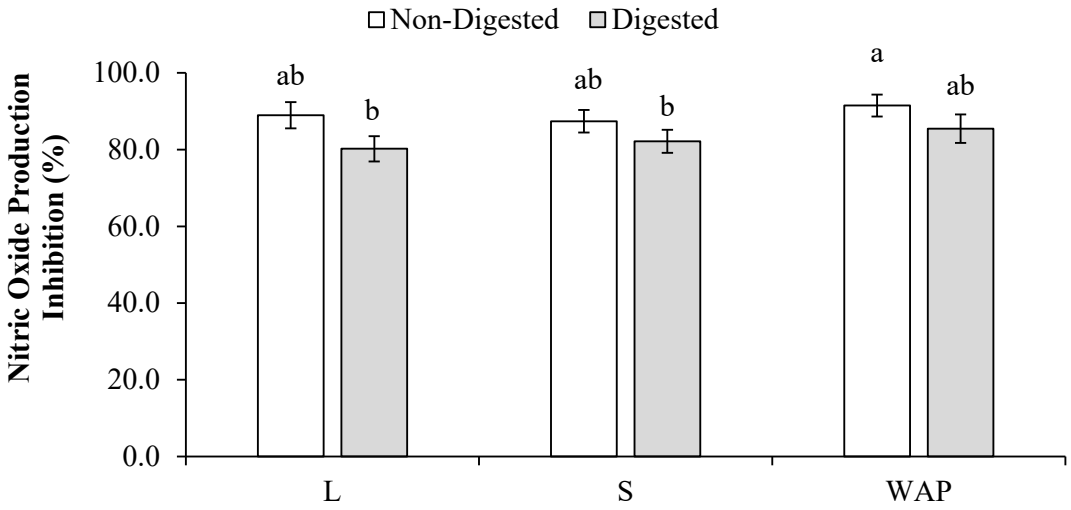

Figure 3. Inhibition of nitric oxide production (%) in murine macrophages (RAW 264.7) cells treated with leaf (L), stem (S), and whole aerial parts (WAP) extracts from *P. brachystachyum*, before (non-digested) and after (digested), submitted to a simulated gastrointestinal digestion. Samples were evaluated at a concentration of 25 µg/mL. Data shown as mean ± standard deviation. [abc] Different letters indicate significant differences between samples determined by Tukey's test ($p < 0.05$).

3.6. In Silico Analysis Results

3.6.1. Drug-Likeness, PASS Analysis, ADMET Properties, and Toxicity Results

The in silico drug-likeness, predicted bioactivity, pharmacokinetic, and toxicity profiles of the selected *Phoradendron brachystachyum* compounds were evaluated to assess their suitability as potential therapeutic candidates. According to Lipinski's Rule of Five, six compounds exhibited more than two violations related to hydrogen bond donors, hydrogen bond acceptors, and topological polar surface area (TPSA), suggesting potential limitations in oral bioavailability (Table S3). Lipinski's criteria indicate that compounds with molecular weight below 500 Da, LogP < 5, fewer than five hydrogen bond donors, and fewer than ten hydrogen bond acceptors are more likely to display favorable oral absorption[61].

These parameters may be associated with reduced absorption, rapid metabolism, or suboptimal distribution, potentially affecting pharmacokinetic performance [62]. However, it is important to note that deviations from Lipinski's rules do not preclude biological activity, particularly for polyphenolic and glycosylated compounds, which often exhibit good bioactivity despite limited oral bioavailability. Therefore, these results were considered as preliminary indicators rather than exclusion criteria.

ADMET predictions further revealed that five compounds showed inhibitory potential against major cytochrome P450 isoforms, including CYP1A2, CYP2C19, CYP2C9, CYP2D6, and CYP3A4. Since these enzymes play a central role in xenobiotic metabolism, their inhibition may lead to altered

© 2026 by the author(s). Distributed under a Creative Commons CC BY license.

Preprints.org (www.preprints.org) | NOT PEER-REVIEWED | Posted: 27 March 2026 doi:10.20944/preprints202603.2241.v1

drug metabolism or potential drug–drug interactions [63], , highlighting the importance of careful pharmacokinetic evaluation in future development stages. Regarding distribution properties, only two compounds were predicted to cross the blood–brain barrier, while six compounds exhibited high gastrointestinal absorption (Table S4), suggesting a preferential peripheral and metabolic mode of action rather than central nervous system activity. Toxicity predictions indicated low acute toxicity risk for the majority of the compounds, supporting their potential as safe bioactive agents. Collectively, these in silico results support the selection of a subset of *P. brachystachyum* compounds for further structure-based analyses, including molecular docking and dynamic simulations.

PASS-based bioactivity predictions revealed a coherent pharmacological profile for the phytochemicals identified in *P. brachystachyum*, with a strong predominance of antioxidant-related activities (Figure 4). Most flavonoids and flavonol glycosides showed high probabilities of activity (Pa > 0.7) as free radical scavengers, antioxidants, and inhibitors of lipid peroxidation and NADPH oxidase, supporting a relevant role in oxidative stress mitigation (Košinová et al., 2011; Tumilaar et al., 2024). Quercetin derivatives, hyperoside, and spiraeoside exhibited the highest Pa values (>0.95) across multiple antioxidant endpoints, consistent with their polyphenolic scaffolds and known redox-modulating capacity (Marrazzo & O'Leary, 2020; Batiha et al., 2020).

In contrast, predictions for carbohydrate-hydrolyzing enzymes revealed a preferential inhibition of α-glucosidase (Pa = 0.70–0.89) over α-amylase, particularly among glycosylated flavonoids. This selective profile suggests a modulation of postprandial glucose absorption with potentially fewer gastrointestinal effects (J. Zhu et al., 2019; Proença et al., 2021) Although sakuranetin and quercetin aglycone displayed low PASS-predicted α-amylase inhibition, their favorable binding energies observed in docking analyses indicate stable enzyme interactions. This divergence reflects the methodological differences between PASS, which relies on structure–activity precedents, and docking simulations, which evaluate physicochemical binding feasibility. The comprehensive in silico research substantiates the multitarget antidiabetic potential of *P. brachystachyum*, principally facilitated by antioxidant pathways and selective α-glucosidase inhibition.

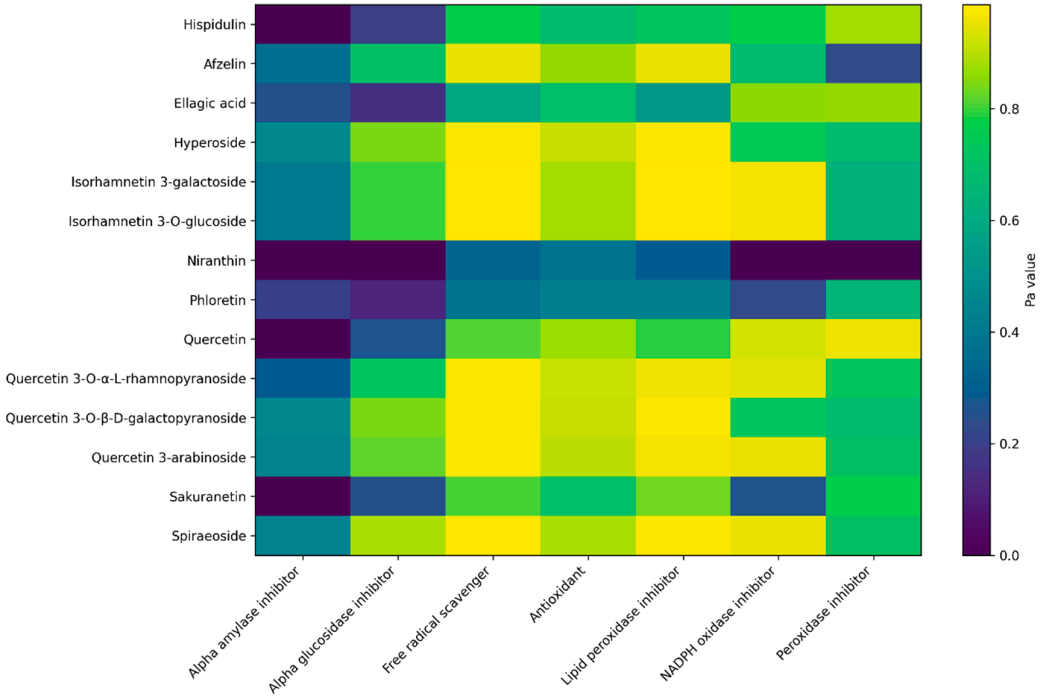

Figure 4. Heatmap representation of the predicted biological activities of *P. brachystachyum* compounds based on PASS analysis. The heatmap summarizes the probability of activity (Pa) values for seven relevant bioactivities associated with antidiabetic and antioxidant mechanisms, including α-amylase inhibition, α-glucosidase

© 2026 by the author(s). Distributed under a Creative Commons CC BY license.

Preprints.org (www.preprints.org) | NOT PEER-REVIEWED | Posted: 27 March 2026 doi:10.20944/preprints202603.2241.v1

inhibition, free radical scavenging, antioxidant activity, lipid peroxidase inhibition, NADPH oxidase inhibition, and peroxidase inhibition. Color intensity reflects increasing Pa values, highlighting compounds with multitarget potential and strong antioxidant-related profiles. This visualization emphasizes the contribution of oxidative stress modulation and enzyme inhibition to the predicted antidiabetic effects of the evaluated phytochemicals.

The in silico toxicity predictions indicated that none of the evaluated compounds exhibited alerts related to hepatotoxicity, neurotoxicity, or general cytotoxicity. In contrast, the models predicted a potential association with nephrotoxicity and respiratory toxicity endpoints for all compounds, which should be interpreted as preliminary risk signals derived from structure–activity relationships rather than definitive toxic effects. Importantly, all compounds were classified within toxicity classes III, IV, and V, corresponding to low acute toxicity risk according to the ProTox-II classification system (Table S6).

The overall low predicted toxicity profile supports the pharmacological feasibility of these compounds as bioactive candidates. Nevertheless, the presence of predicted organ-specific toxicity alerts underscores the need for further experimental validation and structural optimization to improve safety margins. Future studies should focus on refining the pharmacokinetic and toxicological properties of these compounds through in vitro and in vivo assays, with the aim of enhancing efficacy while minimizing potential adverse effects. Collectively, these findings suggest that *P. brachystachyum* compounds represent promising scaffolds for the development of safer and more effective therapeutic agents.

3.6.2. Molecular Docking Analysis

Molecular docking analyses revealed that sakuranetin and spiraeoside exhibited the most favorable binding affinities toward the α-amylase enzyme, with predicted binding free energies of −9.0 kcal·mol^{-1} for both compounds (Figure 5A,B). In the case of α-glucosidase, quercetin 3-O-α-L-rhamnopyranoside and spiraeoside showed the highest binding affinities, each with a binding energy of −9.9 kcal·mol^{-1} (Figure 5C,D). These results suggest that these compounds possess a strong propensity to interact with key carbohydrate-hydrolyzing enzymes involved in glucose metabolism, supporting their potential relevance in the modulation of postprandial hyperglycemia. [64,65]. The high-affinity binding of these compounds was further supported by the formation of multiple stabilizing interactions within the catalytic regions of the enzymes. In the α-amylase–sakuranetin complex, four conventional hydrogen bonds were observed involving residues Gln63, Tyr62, Asp300, and His305, along with two π–π stacking interactions with Trp59. An unfavorable acceptor–acceptor interaction with Asp197 was also detected. Spiraeoside bound to α-amylase through two conventional hydrogen bonds with Trp59 and Tyr151, one π–σ interaction with Leu162, one π–alkyl interaction with Lys200, two π–π T-shaped interactions with His201, and one unfavorable donor–donor interaction with Ile235. For α-glucosidase, quercetin 3-O-α-L-rhamnopyranoside established three conventional hydrogen bonds with Asp408, Arg312, and Asn412, in addition to one π–π T-shaped interaction with Phe157 and several alkyl and π–alkyl interactions involving His245, Ala278, and His279. An unfavorable donor–donor interaction with His279 was also identified. Spiraeoside formed an extensive interaction network within the α-glucosidase binding pocket, including six conventional hydrogen bonds with Asp349, Phe157, Asp408, Arg312, Phe310, and His270, as well as π–cation interactions with Asp349, π–anion interactions with Arg439, and a π–π T-shaped interaction with Tyr71. One unfavorable donor–donor interaction with His348 was also observed.

Overall, the binding modes of spiraeoside and quercetin 3-O-α-L-rhamnopyranoside within the α-glucosidase active site involved a combination of hydrogen bonding, electrostatic, and aromatic interactions, highlighting the complexity of the molecular recognition processes governing ligand–enzyme association (Baron & McCammon, 2013). The presence of both favorable and unfavorable interactions reflects the dynamic balance of forces contributing to binding affinity and specificity.

© 2026 by the author(s). Distributed under a Creative Commons CC BY license.

Preprints.org (www.preprints.org) | NOT PEER-REVIEWED | Posted: 27 March 2026 doi:10.20944/preprints202603.2241.v1

Detailed binding energy values and interacting residues for all ligand–receptor complexes are summarized in Tables 2 and 3.

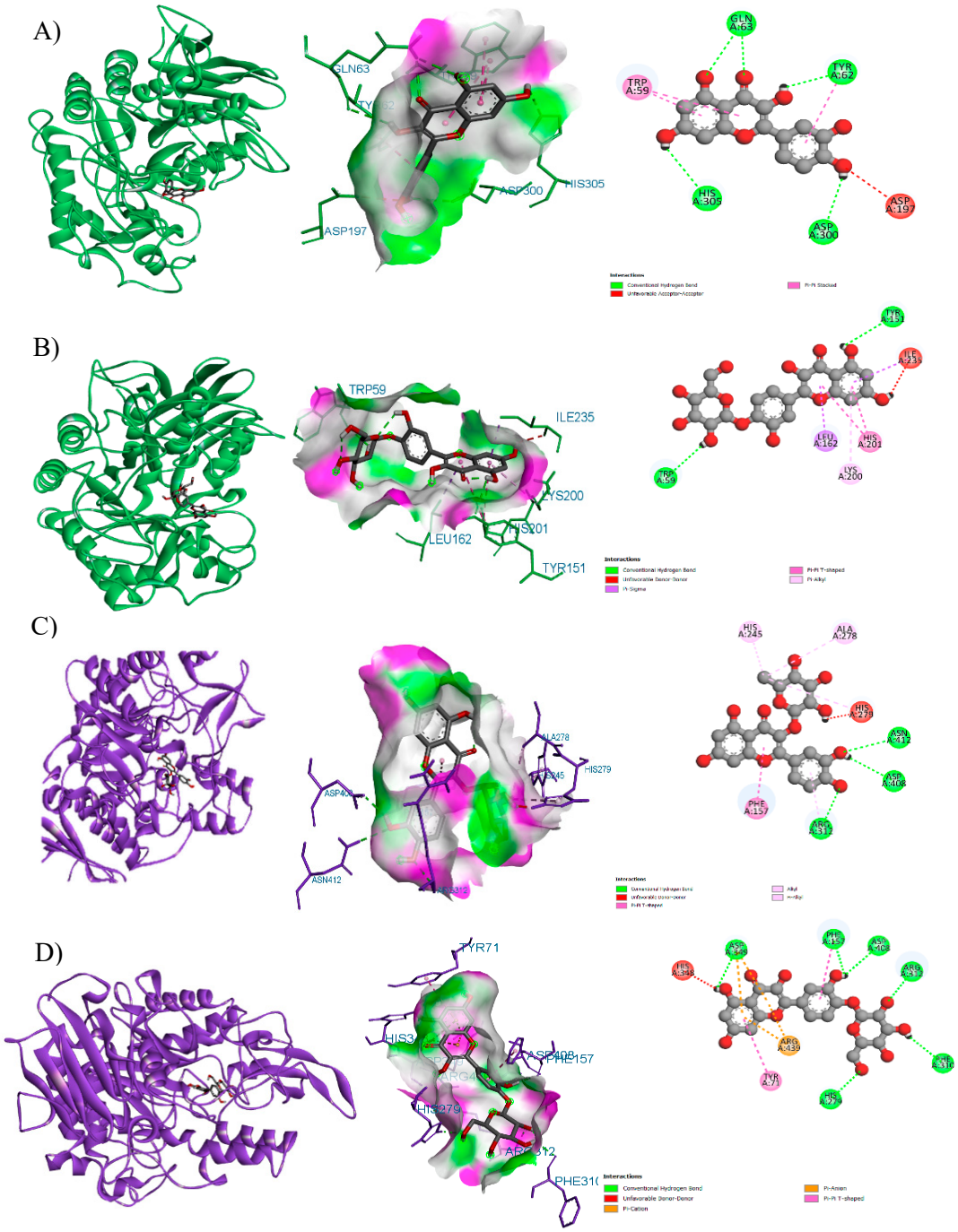

Figure 5. (A) Three-dimensional representation of α-amylase in complex with sakuranetin, highlighting the ligand binding pose and key interactions within the catalytic pocket. (B) α-Amylase–spiraeoside complex showing the binding orientation and principal ligand–receptor interactions. (C) Docked complex of α-glucosidase with quercetin 3-O-α-L-rhamnopyranoside, illustrating the ligand accommodation within the active site. (D) α-Glucosidase–spiraeoside complex depicting the binding mode and stabilizing interactions at the enzyme active region.

Table 2. Binding energies and interacting amino acids between the compounds of *P. brachystachyum and* α-amylase. Docking interactions with the best binding energies are highlighted in blue.

© 2026 by the author(s). Distributed under a Creative Commons CC BY license.

Preprints.org (www.preprints.org) | NOT PEER-REVIEWED | Posted: 27 March 2026 doi:10.20944/preprints202603.2241.v1

Ligands	Receptor proteins	Binding energy (kca mol^{-1})	Interacting amino acid residues
Afzelin	α-amylase	-8.2	Trp58, Ile235, Lys200, Leu162, His305, Glu233, Asp197
Ellagic Acid	α-amylase	-8.3	Phe348, Ala310, Asp317, Arg267, Thr314, Arg346
Hispidulin	α-amylase	-8.7	Gln63, Arg195, His299, Tyr62, Trp59
Hyperoside	α-amylase	-8.3	Ser163, Leu165, Tyr62, Asp300, Arg195, Asp197, Glu233
Isorhamnetin 3-galactoside	α-amylase	-8.1	Tyr151, Ile235, Leu162, His305, Glu233, Arg195, Asp197, His299
Isorhamnetin 3-o-glucoside	α-amylase	-8.2	Ile235, Lys200, Leu162, Ser163, Arg195, Asp197, Asp300
Niranthin	α-amylase	-6.5	His101, Leu162, Trp52, Leu165, His299, Asp197, Tyr62, Gln63
Phloretin	α-amylase	-7.3	Ala198, Glu233, Asp197, Trp59
Quercetin 3-arabinoside	α-amylase	-8	Arg195, Tyr62, Asp300, Leu165, Glu233, Gly306, His299
Quercetin 3-O-alpha-L-rhamnopyranoside	α-amylase	-8.2	Leu162, Ile235, Lys200, Trp58, Asp197
Quercetin	α-amylase	-8.3	Trp59, His305, Asp300, Asp197, Tyr62, Gln63
Quercetin-3-O-beta-D-galactopyranoside	α-amylase	-8.2	Ser163, Leu162, Ile235, Lys200, Asp300, Asp197, Arg195, His305
Sakuranetin	α-amylase	-9	Gln63, Tyr62, Asp300, His305, Trp59
Spiraeoside	α-amylase	-9	Trp59, Leu162, Lys200, His201, Ile235, Tyr151

Table 3. Binding energies and interacting amino acids between the compounds of *P. Brachystachyum and* α-glucosidase. Highlighted in blue are the docking interactions with the best binding energies.

Ligands	Receptor protein	Binding energies (kcal mol^{-1})	Interacting amino acid residues
Afzelin	α-glucosidase	-9.3	Tyr71, Phe177, Glu276, Ala278, Thr215, Arg312
Ellagic Acid	α-glucosidase	-8.8	Arg312, Arg439, Ala278, Phe157
Hispidulin	α-glucosidase	-8.4	Phe311, His239, Asp408, Asp349, Phe157, Phe177, Arg312
Hyperoside	α-glucosidase	-9	Arg439, Asp349, Glu276, Asn241, Glu304, Arg312, Lys155
Isorhamnetin 3-galactoside	α-glucosidase	-8.6	Glu276, Asp349, Arg439, Tyr71, Phe158, Phe157, Arg312
Isorhamnetin 3-o-glucoside	α-glucosidase	-9	Arg312, Pro309, His239, Phe157, Ala278, Asn241, His279, Glu304, Phe311

© 2026 by the author(s). Distributed under a Creative Commons CC BY license.

Preprints.org (www.preprints.org) | NOT PEER-REVIEWED | Posted: 27 March 2026 doi:10.20944/preprints202603.2241.v1

Niranthin	α-glucosidase	-7.2	His348, Asp408, Arg312, Asp349, Tyr71, Arg439, Asp214, Asp68, Glu276
Phloretin	α-glucosidase	-8.2	Pro309, Asn241, Arg312
Quercetin 3-arabinoside	α-glucosidase	-8.5	His245, Ala278, His279, Asn412, Asp408, Arg312, Phe157
Quercetin 3-O-alpha-L-rhamnopyranoside	α-glucosidase	-9.9	His245, Ala278, His279, Asn412, Asp408, Arg312, Phe157
Quercetin	α-glucosidase	-8.9	His279, Arg439, Glu276, Asp349, Phe300, Phe157, Ala278
Quercetin-3-O-beta-D-galactopyranoside	α-glucosidase	-9.7	His279, Arg439, Glu276, Asp349, Phe300, Phe157, Ala278
Sakuranetin	α-glucosidase	-8.5	Arg312, Asp214, Tyr71, Phe177, Gln181, His111, Arg439, Asp349
Spiraeoside	α-glucosidase	-9.9	His348, Asp349, Phe157, Asp408, Arg312, Phe310, His279, Arg439, Tyr71

3.6.3. Molecular Dynamics Simulation

Results for dynamic simulations of the four protein-ligand complexes are presented independently in **Figures S4–S7**. According to the RMSD, good stability was observed for the ligands spiraeoside (α-glucosidase) and sakuranetin, and for spiraeoside (α-amylase), considering a RMSD below 2 Å (0.2 nm) as the criterion. For the ligand quercetin, 3-O-alpha-L-rhamnopyranoside moderate values were obtained. RMSF allows the quantification of the average fluctuations in the positions of atoms within the molecule over time. Our results indicate low flexibility of the backbone atoms in all four complexes throughout the 100 ns analyzed, suggesting that the atoms maintain adequate rigidity within the protein. High flexibility was observed only at the beginning of the experiment for the metabolites spiraeoside (**Figure S4B**) and quercetin 3-O-alpha-L-rhamnopyranoside (**Figure S5B**) in relation to protein α-glucosidase. However, as the analysis progressed, the atoms achieved stability immediately after atom 200, considering that the protein consisted of almost 9,000 atoms. Based on the radius of gyration, the ligand complexes displayed values close to 0.5 nm, indicating a compact structure due to the small size of the metabolites. In contrast, both the protein and its backbone exhibited higher values, up to 2.5 nm, suggesting a more extended structure, consistent with the large size of the α-glucosidase and α-amylase proteins, which contain over 8,500 atoms. Regarding potential energy, the metabolites associated with α-glucosidase obtained similar values ranging from-8.28e+05 to -8.22e+05, while those associated with α-amylase also showed comparable results (-6.64e+05 to -6.58e05+). This is primarily due to the structural differences between α-amylase and α-glucosidase. Given the growing importance of using plant metabolites as alternatives to synthetic drugs, there is increasing interest in in silico studies evaluating α-amylase and α-glucosidase as strategies for diabetes treatment [66–68]. In this context, several authors have studied the conformational stability of complexes of proteins with metabolites such as epicatechin, quercetin, luteolin, and acarbose, among others [69–72]. Although our study revisits some of these metabolites, it is important to note that our molecular dynamics simulation extended over 100 ns, whereas other studies range from 30 to 50 ns [73]. Longer simulations, such as those used in our study, provide a clear perspective on the conformational stability of the molecules.

© 2026 by the author(s). Distributed under a Creative Commons CC BY license.

Preprints.org (www.preprints.org) | NOT PEER-REVIEWED | Posted: 27 March 2026 doi:10.20944/preprints202603.2241.v1

Complementing this information, the results of our molecular dynamics analysis, expressed as conformational stability, support the idea that quercetin could be a promising candidate for treating diabetes mellitus. This finding aligns with those reported by previous studies about this metabolite [70,71]. When comparing the in silico stability of our four complexes with other complexes (same proteins) involving metabolites such as acarbose and apigenin [69], we found that our complexes exhibited lower RMSD and RMSF values. These criteria are crucial for assessing the stability of the complex, suggesting that the complexes analyzed in this study show superior pharmacological potential. However, among the metabolites, we recommend in vitro evaluations of quercetin 3-O-alpha-L-rhamnopyranoside for α-glucosidase and sakuranetin for α-amylase.

4. Conclusions

This research has shown that Toji mistletoe (*P. brachystachyum*) exhibits greater cellular antioxidant activity by inhibiting peroxyl radicals, strong anti-inflammatory potential by inhibiting nitric oxide production, and improved glucose uptake by liver cells under insulin-resistant conditions, suggesting a reversal effect of this condition. In the quantification of the phenolic compounds present in the extracts, three compounds were identified: quercetin-3-O-rhamnoside, rutin, and hesperidin, with quercetin-3-O-rhamnoside being the most abundant in both digested and non-digested extracts. No differences in biological activity were observed among Toji extracts, regardless of the plant section used to make the extract. As expected, gastrointestinal digestion significantly reduced the quercetin-3-O-rhamnoside, rutin, and hesperidin content in all extracts. Likewise, glucose uptake in insulin-resistant cells treated with leaf (L), stem (S), and whole aerial parts (WAP) extracts, and cellular antioxidant activity of cells treated with WAP extract, were reduced after digestion, with no differences observed between treatments. In contrast, the anti-inflammatory potential was unaffected by digestion or by the type of extract used, possibly because of the high levels of glycosylated flavonoids, which tend to be more resistant to digestion and whose activity is mainly associated with the release of their aglycone. The most relevant effect of toji extracts was a significant improvement in glucose uptake in insulin-resistant liver cells, even at levels comparable to those of glibenclamide, a commercial drug. Although this effect was significantly reduced after digestion of the extracts, it showed significant improvement compared to the control of untreated insulin-resistant cells. Finally, an integrated in silico assessment was performed on 14 compounds previously identified in *Phoradendron brachystachyum* to systematically evaluate their drug-likeness, pharmacokinetic behavior, and interaction potential with key carbohydrate-hydrolyzing enzymes. This computational approach enabled the prioritization of bioactive candidates by combining ADMET profiling with structure-based analyses, revealing that sakuranetin, spiraeoside, and quercetin 3-O-α-L-rhamnopyranoside exhibited the most favorable binding energies and stable interaction patterns with α-amylase and α-glucosidase. These findings highlight the relevance of in silico methodologies as efficient and cost-effective tools for narrowing down promising phytochemicals prior to experimental validation. Overall, the Toji mistletoe (*P. brachystachyum*) demonstrated notable biological potential, supporting its traditional use and positioning it as a promising source of compounds capable of modulating metabolic pathways associated with type 2 diabetes. Nevertheless, further mechanistic, pharmacokinetic, and toxicological studies are required to fully elucidate the modes of action, optimize dosing strategies, and assess long-term efficacy and safety. In this context, the present in silico framework provides a robust foundation for guiding future experimental studies and advancing the rational development of Toji-derived compounds as potential alternatives or complements to current antidiabetic therapies.

Supplementary Materials: The following supporting information can be downloaded at website of this paper posted on Preprints.org.

Author Contributions: LAMI: Investigation, methodology, writing – original draft. LIGP: Methodology, writing – original draft, writing, review, and editing. JRAS: Methodology, writing, review, and editing. EOH: Methodology. JBH, writing, review, and editing. JRGG: Writing – review and editing. PJBB: Methodology. JAMF:

© 2026 by the author(s). Distributed under a Creative Commons CC BY license.

Preprints.org (www.preprints.org) | NOT PEER-REVIEWED | Posted: 27 March 2026 doi:10.20944/preprints202603.2241.v1

Methodology, writing – review and editing. LACB: writing – review and editing. MAR: Conceptualization, resources, supervision, writing, review, and editing. EPGG: Conceptualization, resources, supervision, writing, review, and editing.

Funding: L.A.M.I. was supported by a PhD scholarship (792411) from the Secretaría de Ciencia, Humanidades, Tecnología e Innovación (SECIHTI) and an academic stay scholarship from the Centro de Investigación en Alimentación y Desarrollo A.C. The authors thank SECIHTI for the graduate studies scholarship.

Institutional Review Board Statement: Not applicable.

Informed Consent Statement: Not applicable.

Data Availability Statement: The raw data supporting the conclusions of this article will be made available by the authors on request.

Conflicts of Interest: The authors declare no conflicts of interest.

Abbreviations

The following abbreviations are used in this manuscript:

AAPH	2,2′-azobis-2-methylpropanimidamide dihydrochloride
ADMET	Absorption, distribution, metabolism, excretion, and toxicity
CAA	Cellular Antioxidant Activity
CTRL IR	Insulin-resistance control
CTRL Normal	Non-insulin-resistant or normal control
D	Digested
DCFH-DA	2′,7′-dichlorodihydrofluorescein diacetate
DMEM	Dulbecco's Modified Eagle Medium
ECG	Epicatechin-3-gallate
EGCG	Epigallocatechin 3-gallate / Epigallocatechin gallate
ERK	Extracellular signal-regulated kinases
FBS	Fetal bovine serum
IKK	IκB kinase
IR	Insulin-resistant
L	Leaves / leaf
LPS	Lipopolysaccharide
MAPK	Mitogen-activated protein kinase
MD	Molecular dynamics
MW	Molecular weight
NADPH	Nicotinamide adenine dinucleotide phosphate
NCD	Non-communicable disease
ND	Non-digested
NF-κB	Nuclear factor-kappa B
NO	Nitric oxide
NPT	Constant number, pressure, and temperature
NVT	Constant number, volume, and temperature
Pa	Probabilities of activity
PASS	Prediction of Activity Spectra for Substances
PBS	Phosphate-buffered saline
Pi	Probability of inactivity
QSAR	Quantitative structure–activity relationship
Rg	Radius of gyration

© 2026 by the author(s). Distributed under a Creative Commons CC BY license.

Preprints.org (www.preprints.org) | NOT PEER-REVIEWED | Posted: 27 March 2026 doi:10.20944/preprints202603.2241.v1

RMSD	Root mean square deviation
RMSF	Root mean square fluctuation
ROS	Reactive oxygen species
S	Stems / stem
TPSA	Topological polar surface area
WAP	Whole aerial parts

References

1. Cho, N.; Shaw, J.; Karuranga, S.; Huang, Y.; da Rocha Fernandes, J.; Ohlrogge, A.; Malanda, B. IDF Diabetes Atlas: Global estimates of diabetes prevalence for 2017 and projections for 2045. *Diabetes Res. Clin. Pract.* **2018**, *138*, 271-281.
2. International Diabetes Federation. Mexico. Available online: https://idf.org/es/our-network/regions-and-members/south-and-central-america/members/mexico/ (accessed on 10 November).
3. Halliwell, B.; Gutteridge, J.M. *Free radicals in biology and medicine*, 5 ed.; Oxford University Press, USA: 2015.
4. Huang, Q.; Chen, L.; Teng, H.; Song, H.; Wu, X.; Xu, M. Phenolic compounds ameliorate the glucose uptake in HepG2 cells' insulin resistance via activating AMPK: anti-diabetic effect of phenolic compounds in HepG2 cells. *J. Funct. Foods* **2015**, *19*, 487-494, doi:https://doi.org/10.1016/j.jff.2015.09.020.
5. Prabhakar, S.S. Role of nitric oxide in diabetic nephropathy. In Proceedings of the Seminars in nephrology, 2004; pp. 333-344.
6. Donath, M.Y.; Ehses, J.A. Type 1, type 1.5, and type 2 diabetes: NOD the diabetes we thought it was. *Proc. Natl. Acad. Sci. U.S.A.* **2006**, *103*, 12217-12218, doi:https://doi.org/10.1073/pnas.0605480103.
7. Noor, A.; Gunasekaran, S.; Manickam, A.S.; Vijayalakshmi, M.A. Antidiabetic activity of Aloe vera and histology of organs in streptozotocin-induced diabetic rats. *Curr. Sci.* **2008**, 1070-1076, doi:https://www.jstor.org/stable/24100806
8. Halberstein, R.A. Medicinal plants: historical and cross-cultural usage patterns. *Ann. Epidemiol.* **2005**, *15*, 686-699, doi:https://doi.org/10.1016/j.annepidem.2005.02.004.
9. Gil-Rodriguez, J.R.; Herrera-Rojas, M.F.; Mitre-Velasco, Y.; Santamaria-Rivas, C. COMPUESTOS ACTIVOS EN PLANTAS UTILIZADAS EN LA MEDICINA TRADICIONAL MEXICANA. *RD-ICUAP* **2020**, *6*, 175-200.
10. Salehi, B.; Ata, A.; Kumar, N.V.A.; Sharopov, F.; Ramirez-Alarcon, K.; Ruiz-Ortega, A.; Ayatollahi, S.A.; Fokou, P.V.T.; Kobarfard, F.; Zakaria, Z.A.; et al. Antidiabetic Potential of Medicinal Plants and Their Active Components. *Biomolecules* **2019**, *9*, doi:10.3390/biom9100551.
11. Gómez-Sánchez, M.; Sánchez-Fuentes, L.J.; Salazar-Olivo, L.A. Anatomía de especies mexicanas de los géneros Phoradendron y Psittacanthus, endémicos del Nuevo Mundo. *Rev. Mex. Biodivers.* **2011**, *82*, 1203-1218.
12. Lara-Ponce, E., & Quintero-Romanillo. PLANTAS MEDICINALES DEL NORTE DE SINALOA. Los Mochis, Sinaloa, Mexico; 2016.
13. Ramirez-Espinosa, J.J.; Garcia-Jimenez, S.; Rios, M.Y.; Medina-Franco, J.L.; Lopez-Vallejo, F.; Webster, S.P.; Binnie, M.; Ibarra-Barajas, M.; Ortiz-Andrade, R.; Estrada-Soto, S. Antihyperglycemic and sub-chronic antidiabetic actions of morolic and moronic acids, in vitro and in silico inhibition of 11beta-HSD 1. *Phytomedicine* **2013**, *20*, 571-576, doi:10.1016/j.phymed.2013.01.013.
14. Sánchez Salazar, M.G. Search for bioactive compounds in American mistletoes and their mechanisms of action. 2017.
15. Vasconcellos, C.L.; Vitório, K.C.; Andrade, P.A.; Cambuí, É.V.; Lira, A.F.; Cavalcante, S.C.; Estevam, C.S.; Antoniolli, Â.R.; Thomazzi, S.M. Antinociceptive, anti-inflammatory, and antioxidant properties of Phoradendron piperoides leaves. *Pharm. Biol.* **2009**, *47*, 645-652, doi:https://doi.org/10.1080/13880200902917065.
16. Velderrain-Rodríguez, G.; Palafox-Carlos, H.; Wall-Medrano, A.; Ayala-Zavala, J.; Chen, C.O.; Robles-Sánchez, M.; Astiazaran-García, H.; Alvarez-Parrilla, E.; González-Aguilar, G. Phenolic compounds: their journey after intake. *Food Funct.* **2014**, *5*, 189-197, doi:https://doi.org/10.1039/C3FO60361J

© 2026 by the author(s). Distributed under a Creative Commons CC BY license.

Preprints.org (www.preprints.org) | NOT PEER-REVIEWED | Posted: 27 March 2026 doi:10.20944/preprints202603.2241.v1

17. Brodkorb, A.; Egger, L.; Alminger, M.; Alvito, P.; Assunção, R.; Ballance, S.; Bohn, T.; Bourlieu-Lacanal, C.; Boutrou, R.; Carrière, F. INFOGEST static in vitro simulation of gastrointestinal food digestion. *Nat. Protoc.* **2019**, *14*, 991-1014, doi:https://doi.org/10.1038/s41596-018-0119-1.
18. Gutiérrez-Grijalva, E.P.; Zamudio-Sosa, V.E.; Contreras-Angulo, L.A.; Leyva-López, N.; Heredia, J.B. Bioaccessibility of phenolic compounds from mistletoe infusions and effect of in vitro digestion on its antioxidant and pancreatic lipase inhibitory Activity. *Foods* **2022**, *11*, 3319, doi:https://doi.org/10.3390/foods11213319.
19. Gutiérrez-Grijalva, E.P.; Angulo-Escalante, M.A.; León-Félix, J.; Heredia, J.B. Effect of in vitro digestion on the total antioxidant capacity and phenolic content of 3 species of oregano (Hedeoma patens, Lippia graveolens, Lippia palmeri). *J. Food Sci.* **2017**, *82*, 2832-2839, doi: https://doi.org/10.1111/1750-3841.13954.
20. Meléndez-Martínez, D.; Ortega-Hernández, E.; Reza-Zaldívar, E.E.; Carbajal-Saucedo, A.; Arnaud-Franco, G.; Gatica-Colima, A.; Plenge-Tellechea, L.F.; Antunes-Ricardo, M.; Jacobo-Velázquez, D.A.; Mayolo-Deloisa, K.; et al. Bioprospection of rattlesnake venom peptide fractions with anti-adipose and anti-insulin resistance activity in vitro. *Toxicon: X* **2024**, *24*, 100209, doi:https://doi.org/10.1016/j.toxcx.2024.100209.
21. Picos-Salas, M.A.; Leyva-López, N.; Bastidas-Bastidas, P.d.J.; Antunes-Ricardo, M.; Cabanillas-Bojórquez, L.A.; Angulo-Escalante, M.A.; Heredia, J.B.; Gutiérrez-Grijalva, E.P. Supercritical CO2 extraction of naringenin from Mexican oregano (Lippia graveolens): its antioxidant capacity under simulated gastrointestinal digestion. *Sci. Rep.* **2024**, *14*, 1146, doi:https://doi.org/10.1038/s41598-023-50997-2.
22. SwissADME. SwissADME. Available online: https://swissmodel.expasy.org/ (accessed on
23. Daina, A.; Michielin, O.; Zoete, V. SwissADME: a free web tool to evaluate pharmacokinetics, drug-likeness and medicinal chemistry friendliness of small molecules. *Sci. Rep.* **2017**, *7*, 42717, doi:10.1038/srep42717.
24. Khan, K.M.; Rahim, F.; Wadood, A.; Kosar, N.; Taha, M.; Lalani, S.; Khan, A.; Fakhri, M.I.; Junaid, M.; Rehman, W.; et al. Synthesis and molecular docking studies of potent α-glucosidase inhibitors based on biscoumarin skeleton. *Eur. J. Med. Chem.* **2014**, *81*, 245-252, doi:https://doi.org/10.1016/j.ejmech.2014.05.010.
25. Taha, M.; Shah, S.A.A.; Afifi, M.; Imran, S.; Sultan, S.; Rahim, F.; Khan, K.M. Synthesis, α-glucosidase inhibition and molecular docking study of coumarin based derivatives. *Bioorg. Chem.* **2018**, *77*, 586-592, doi:https://doi.org/10.1016/j.bioorg.2018.01.033.
26. Van Der Spoel, D.; Lindahl, E.; Hess, B.; Groenhof, G.; Mark, A.E.; Berendsen, H.J.C. GROMACS: fast, flexible, and free. *J. Comput. Chem.* **2005**, *26*, 1701-1718.
27. Domínguez-Avila, J.A.; Wall-Medrano, A.; Velderrain-Rodríguez, G.R.; Chen, C.-Y.O.; Salazar-López, N.J.; Robles-Sánchez, M.; González-Aguilar, G.A. Gastrointestinal interactions, absorption, splanchnic metabolism and pharmacokinetics of orally ingested phenolic compounds. *Food and Funct.* **2017**, *8*, 15-38, doi:DOI: 10.1039/C6FO01475E.
28. Makarewicz, M.; Drożdż, I.; Tarko, T.; Duda-Chodak, A. The interactions between polyphenols and microorganisms, especially gut microbiota. *Antioxidants* **2021**, *10*, 188, doi:https://doi.org/10.3390/antiox10020188.
29. Gayoso, L.; Roxo, M.; Cavero, R.Y.; Calvo, M.I.; Ansorena, D.; Astiasarán, I.; Wink, M. Bioaccessibility and biological activity of Melissa officinalis, Lavandula latifolia and Origanum vulgare extracts: Influence of an in vitro gastrointestinal digestion. *J. Funct. Foods* **2018**, *44*, 146-154, doi:https://doi.org/10.1016/j.jff.2018.03.003.
30. Li, Q.; Chen, J.; Li, T.; Liu, C.; Wang, X.; Dai, T.; McClements, D.J.; Liu, J. Impact of in vitro simulated digestion on the potential health benefits of proanthocyanidins from Choerospondias axillaris peels. *Food Res. Int.* **2015**, *78*, 378-387, doi:https://doi.org/10.1016/j.foodres.2015.09.004.
31. Bermúdez-Soto, M.-J.; Tomás-Barberán, F.-A.; García-Conesa, M.-T. Stability of polyphenols in chokeberry (Aronia melanocarpa) subjected to in vitro gastric and pancreatic digestion. *Food Chem.* **2007**, *102*, 865-874, doi:https://doi.org/10.1016/j.foodchem.2006.06.025.
32. Wootton-Beard, P.C.; Moran, A.; Ryan, L. Stability of the total antioxidant capacity and total polyphenol content of 23 commercially available vegetable juices before and after in vitro digestion measured by FRAP, DPPH, ABTS and Folin–Ciocalteu methods. *Food Res. Int.* **2011**, *44*, 217-224, doi:https://doi.org/10.1016/j.foodres.2010.10.033.

© 2026 by the author(s). Distributed under a Creative Commons CC BY license.

Preprints.org (www.preprints.org) | NOT PEER-REVIEWED | Posted: 27 March 2026 doi:10.20944/preprints202603.2241.v1

33. Li, C.X.; Wang, F.R.; Zhang, B.; Deng, Z.Y.; Li, H.Y. Stability and antioxidant activity of phenolic compounds during in vitro digestion. *J. Food Sci.* **2023**, *88*, 696-716, doi:https://doi.org/10.1111/1750-3841.16440.
34. Junaid, M.; Basak, B.; Akter, Y.; Afrose, S.S.; Nahrin, A.; Emran, R.; Shahinozzaman, M.; Tawata, S. Sakuranetin and its therapeutic potentials–A comprehensive review. *Z. Naturforsch. C* **2023**, *78*, 27-48, doi:https://doi.org/10.1515/znc-2022-0024.
35. Spencer, J.P.; Abd El Mohsen, M.M.; Rice-Evans, C. Cellular uptake and metabolism of flavonoids and their metabolites: implications for their bioactivity. *Arch. Biochem. Biophys.* **2004**, *423*, 148-161, doi:https://doi.org/10.1016/j.abb.2003.11.010.
36. Bors, W.; Heller, W.; Michel, C.; Saran, M. [36] Flavonoids as antioxidants: Determination of radical-scavenging efficiencies. In *Methods in enzymology*; Elsevier: 1990; Volume 186, pp. 343-355.
37. Silva, M.M.; Santos, M.R.; Caroço, G.; Rocha, R.; Justino, G.; Mira, L. Structure-antioxidant activity relationships of flavonoids: a re-examination. *Free Radic. Res.* **2002**, *36*, 1219-1227, doi:https://doi.org/10.1080/198-1071576021000016472.
38. Burda, S.; Oleszek, W. Antioxidant and antiradical activities of flavonoids. *J. Agric. Food Chem.* **2001**, *49*, 2774-2779, doi:https://doi.org/10.1021/jf001413m.
39. Lin, C.-L.; Huang, H.-C.; Lin, J.-K. Theaflavins attenuate hepatic lipid accumulation through activating AMPK in human HepG2 cell[ss]. *J. Lipid Res.* **2007**, *48*, 2334-2343, doi:https://doi.org/10.1194/jlr.M700128-JLR200.
40. Wanyo, P.; Chamsai, T.; Toontom, N.; Nghiep, L.K.; Tudpor, K. Differential effects of in vitro simulated digestion on antioxidant activity and bioaccessibility of phenolic compounds in purple rice bran extracts. *MOLECULES* **2024**, *29*, 2994, doi:https://doi.org/10.3390/molecules29132994.
41. Roghani, M.; Baluchnejadmojarad, T. Hypoglycemic and hypolipidemic effect and antioxidant activity of chronic epigallocatechin-gallate in streptozotocin-diabetic rats. *Pathophysiology* **2010**, *17*, 55-59, doi:https://doi.org/10.1016/j.pathophys.2009.07.004.
42. Shisheva, A.; Shechter, Y. Quercetin selectively inhibits insulin receptor function in vitro and the bioresponses of insulin and insulinomimetic agents in rat adipocytes. *Biochemistry* **1992**, *31*, 8059-8063.
43. Nomura, M.; Takahashi, T.; Nagata, N.; Tsutsumi, K.; Kobayashi, S.; Akiba, T.; Yokogawa, K.; Moritani, S.; Miyamoto, K.-i. Inhibitory mechanisms of flavonoids on insulin-stimulated glucose uptake in MC3T3-G2/PA6 adipose cells. *Biol. Pharm. Bull.* **2008**, *31*, 1403-1409, doi:https://doi.org/10.1248/bpb.31.1403.
44. Orhan, D.D.; Senol, F.S.; Hosbas, S.; Orhan, I.E. Assessment of cholinesterase and tyrosinase inhibitory and antioxidant properties of Viscum album L. samples collected from different host plants and its two principal substances. *Ind. Crops Prod.* **2014**, *62*, 341-349, doi:https://doi.org/10.1016/j.indcrop.2014.08.044.
45. Terra, X.; Palozza, P.; Fernandez-Larrea, J.; Ardevol, A.; Blade, C.; Pujadas, G.; Salvado, J.; Arola, L.; Blay, M.T. Procyanidin dimer B1 and trimer C1 impair inflammatory response signalling in human monocytes. *Free Radic. Res.* **2011**, *45*, 611-619, doi:https://doi.org/10.3109/10715762.2011.564165.
46. Terra, X.; Valls, J.; Vitrac, X.; Mérrillon, J.-M.; Arola, L.; Ardèvol, A.; Bladé, C.; Fernández-Larrea, J.; Pujadas, G.; Salvadó, J. Grape-seed procyanidins act as antiinflammatory agents in endotoxin-stimulated RAW 264.7 macrophages by inhibiting NFkB signaling pathway. *J. Agric. Food Chem.* **2007**, *55*, 4357-4365, doi:https://doi.org/10.1021/jf0633185.
47. Nishi, K.; Oda, T.; Takabuchi, S.; Oda, S.; Fukuda, K.; Adachi, T.; Semenza, G.L.; Shingu, K.; Hirota, K. LPS induces hypoxia-inducible factor 1 activation in macrophage-differentiated cells in a reactive oxygen species–dependent manner. *Antioxid. Redox Signal.* **2008**, *10*, 983-996, doi:https://doi.org/10.1089/ars.2007.1825.
48. Ryan, K.A.; Smith Jr, M.F.; Sanders, M.K.; Ernst, P.B. Reactive oxygen and nitrogen species differentially regulate Toll-like receptor 4-mediated activation of NF-κB and interleukin-8 expression. *Infect. Immun.* **2004**, *72*, 2123-2130, doi:https://doi.org/10.1128/iai.72.4.2123-2130.2004.
49. Bonizzi, G.; Piette, J.; Merville, M.-P.; Bours, V. Cell type-specific role for reactive oxygen species in nuclear factor-kappaB activation by interleukin-1. *Biochem. Pharmacol.* **2000**, *59*, 7-11, doi:https://doi.org/10.1016/S0006-2952(99)00290-7.

© 2026 by the author(s). Distributed under a Creative Commons CC BY license.

Preprints.org (www.preprints.org) | NOT PEER-REVIEWED | Posted: 27 March 2026 doi:10.20944/preprints202603.2241.v1

50. Mackenzie, G.G.; Carrasquedo, F.; Delfino, J.M.; Keen, C.L.; Fraga, C.G.; Oteiza, P.I. Epicatechin, catechin, and dimeric procyanidins inhibit PMA-induced NF-B activation at multiple steps in Jurkat T cells. **2003**.
51. Nagai, H.; Noguchi, T.; Takeda, K.; Ichijo, H. Pathophysiological roles of ASK1-MAP kinase signaling pathways. *BMB Rep.* **2007**, *40*, 1-6.
52. Weiss, T.; Shalit, I.; Blau, H.; Werber, S.; Halperin, D.; Levitov, A.; Fabian, I. Anti-inflammatory effects of moxifloxacin on activated human monocytic cells: inhibition of NF-κB and mitogen-activated protein kinase activation and of synthesis of proinflammatory cytokines. *Antimicrob. Agents Chemother.* **2004**, *48*, 1974-1982, doi:https://doi.org/10.1128/aac.48.6.1974-1982.2004.
53. Verhaeghe, C.; Remouchamps, C.; Hennuy, B.; Vanderplasschen, A.; Chariot, A.; Tabruyn, S.P.; Oury, C.; Bours, V. Role of IKK and ERK pathways in intrinsic inflammation of cystic fibrosis airways. *Biochem. Pharmacol.* **2007**, *73*, 1982-1994, doi:https://doi.org/10.1016/j.bcp.2007.03.019.
54. Suh, S.-J.; Chung, T.-W.; Son, M.-J.; Kim, S.-H.; Moon, T.C.; Son, K.H.; Kim, H.P.; Chang, H.W.; Kim, C.-H. The naturally occurring biflavonoid, ochnaflavone, inhibits LPS-induced iNOS expression, which is mediated by ERK1/2 via NF-κB regulation, in RAW264. 7 cells. *Arch. Biochem. Biophys.* **2006**, *447*, 136-146, doi:https://doi.org/10.1016/j.abb.2006.01.016.
55. Gloire, G.; Legrand-Poels, S.; Piette, J. NF-κB activation by reactive oxygen species: fifteen years later. *Biochem. Pharmacol.* **2006**, *72*, 1493-1505, doi:https://doi.org/10.1016/j.bcp.2006.04.011.
56. Park, H.S.; Jung, H.Y.; Park, E.Y.; Kim, J.; Lee, W.J.; Bae, Y.S. Cutting edge: direct interaction of TLR4 with NAD (P) H oxidase 4 isozyme is essential for lipopolysaccharide-induced production of reactive oxygen species and activation of NF-κB. *J. Immunol.* **2004**, *173*, 3589-3593, doi:https://doi.org/10.4049/jimmunol.173.6.3589.
57. Steffen, Y.; Gruber, C.; Schewe, T.; Sies, H. Mono-O-methylated flavanols and other flavonoids as inhibitors of endothelial NADPH oxidase. *Arch. Biochem. Biophys.* **2008**, *469*, 209-219, doi:https://doi.org/10.1016/j.abb.2007.10.012.
58. Delehanty, J.B.; Johnson, B.J.; Hickey, T.E.; Pons, T.; Ligler, F.S. Binding and neutralization of lipopolysaccharides by plant proanthocyanidins. *J. Nat. Prod.* **2007**, *70*, 1718-1724, doi:https://doi.org/10.1021/np0703601.
59. Hong, M.H.; Kim, M.H.; Chang, H.J.; Kim, N.H.; Shin, B.A.; Ahn, B.W.; Jung, Y.D. (−)-Epigallocatechin-3-gallate inhibits monocyte chemotactic protein-1 expression in endothelial cells via blocking NF-κB signaling. *Life Sci.* **2007**, *80*, 1957-1965, doi:https://doi.org/10.1016/j.lfs.2007.02.024.
60. Mackenzie, G.G.; Delfino, J.M.; Keen, C.L.; Fraga, C.G.; Oteiza, P.I. Dimeric procyanidins are inhibitors of NF-κB–DNA binding. *Biochem. Pharmacol.* **2009**, *78*, 1252-1262, doi:https://doi.org/10.1016/j.bcp.2009.06.111.
61. Karami, T.K.; Hailu, S.; Feng, S.; Graham, R.; Gukasyan, H.J. Eyes on Lipinski's Rule of Five: A New "Rule of Thumb" for Physicochemical Design Space of Ophthalmic Drugs. *J. Ocul. Pharmacol. Ther.* **2021**, *38*, 43-55, doi:10.1089/jop.2021.0069.
62. Hou, T.; Wang, J.; Zhang, W.; Xu, X. ADME Evaluation in Drug Discovery. 7. Prediction of Oral Absorption by Correlation and Classification. *J. Chem. Inf. Model.* **2007**, *47*, 208-218, doi:10.1021/ci600343x.
63. Qiu, J.-X.; Zhou, Z.-W.; He, Z.-X.; Zhang, X.; Zhou, S.-F.; Zhu, S. Estimation of the binding modes with important human cytochrome P450 enzymes, drug interaction potential, pharmacokinetics, and hepatotoxicity of ginger components using molecular docking, computational, and pharmacokinetic modeling studies. *Drug Des. Devel. Ther.* **2015**, 841-866, doi:DOI: 10.2147/DDDT.S74669.
64. Dowarah, J.; Singh, V.P. Anti-diabetic drugs recent approaches and advancements. *Bioorg. Med. Chem.* **2020**, *28*, 115263, doi:https://doi.org/10.1016/j.bmc.2019.115263.
65. Zhu, Y.; Zhao, J.; Luo, L.; Gao, Y.; Bao, H.; Li, P.; Zhang, H. Research progress of indole compounds with potential antidiabetic activity. *Eur. J. Med. Chem.* **2021**, *223*, 113665, doi:https://doi.org/10.1016/j.ejmech.2021.113665.
66. Kajaria, D.; Tripathi, J.; Tripathi, Y.B.; Tiwari, S. In-vitro α amylase and glycosidase inhibitory effect of ethanolic extract of antiasthmatic drug—Shirishadi. *J. Adv. Pharm. Technol. Res.* **2013**, *4*, 206-209.
67. Ojah, E.O.; Moronkola, D.O.; Akintunde, A.-A.M. α-amylase and α-glucosidase antidiabetic potential of ten essential oils from Calophyllum inophyllum Linn. *Iberoam. J. Med.* **2020**, *2*, 253-260.

© 2026 by the author(s). Distributed under a Creative Commons CC BY license.

Preprints.org (www.preprints.org) | NOT PEER-REVIEWED | Posted: 27 March 2026 doi:10.20944/preprints202603.2241.v1

68. Li, X.; Bai, Y.; Jin, Z.; Svensson, B. Food-derived non-phenolic α-amylase and α-glucosidase inhibitors for controlling starch digestion rate and guiding diabetes-friendly recipes. *LWT* **2022**, *153*, 112455.
69. Ahmed, S.; Ali, M.C.; Ruma, R.A.; Mahmud, S.; Paul, G.K.; Saleh, M.A.; Alshahrani, M.M.; Obaidullah, A.J.; Biswas, S.K.; Rahman, M.M. Molecular docking and dynamics simulation of natural compounds from betel leaves (Piper betle L.) for investigating the potential inhibition of alpha-amylase and alpha-glucosidase of type 2 diabetes. *MOLECULES* **2022**, *27*, 4526.
70. Kikiowo, B.; Ahmad, I.; Alade, A.A.; T. Ijatuyi, T.; Iwaloye, O.; Patel, H.M. Molecular dynamics simulation and pharmacokinetics studies of ombuin and quercetin against human pancreatic α-amylase. *J. Biomol. Struct. Dyn.* **2023**, *41*, 10388-10395.
71. Mohamed, G.A.; Omar, A.M.; El-Araby, M.E.; Mass, S.; Ibrahim, S.R.M. Assessments of alpha-amylase inhibitory potential of tagetes flavonoids through in vitro, molecular docking, and molecular dynamics simulation studies. *Int. J. Mol. Sci.* **2023**, *24*, 10195.
72. Oyewusi, H.A.; Wu, Y.-S.; Safi, S.Z.; Wahab, R.A.; Hatta, M.H.M.; Batumalaie, K. Molecular dynamics simulations reveal the inhibitory mechanism of Withanolide A against α-glucosidase and α-amylase. *J. Biomol. Struct. Dyn.* **2023**, *41*, 6203-6218.
73. Sharma, P.; Joshi, T.; Joshi, T.; Chandra, S.; Tamta, S. Molecular dynamics simulation for screening phytochemicals as α-amylase inhibitors from medicinal plants. *J. Biomol. Struct. Dyn.* **2021**, *39*, 6524-6538.

Disclaimer/Publisher's Note: The statements, opinions and data contained in all publications are solely those of the individual author(s) and contributor(s) and not of MDPI and/or the editor(s). MDPI and/or the editor(s) disclaim responsibility for any injury to people or property resulting from any ideas, methods, instructions or products referred to in the content.

© 2026 by the author(s). Distributed under a Creative Commons CC BY license.